Preliminary Experiments of Faceted Cellular Array Growth in Microgravity

Yuko INATOMI[1], Kayoko IWAMOTO[2], Takao MAKI[3], Yoshiki TAKAGI[2], and Kazuhiko KURIBAYASHI[1]

[1] Japan Aerospace Exploration Agency, Sagamihara, Kanagawa, Japan, inatomi@isas.jaxa.jp
[2] Teikyo University of Science and Technology, Uenohara, Yamanashi, Japan
[3] Olympus Optical Co., Hachioji, Tokyo, Japan

Abstract

In situ observation experiments of faceted cellular growth will be carried out in transparent organic alloy, salol - t-butyl alcohol in microgravity conditions using a sounding rocket and the International Space Station. The growth rate and the profiles of temperature and solute concentration in the vicinity of the solid-liquid interface will be simultaneously measured by microscopic interferometers in order to evaluate the morphological instability taking account of released latent heat in faceting material.

1. Introduction

Some works on production of high quality semiconductor devices, for example thin-film silicon single crystals produced by zone melting recrystallization, have reported break-down from a planar solid-liquid (S/L) interface to a faceted cellular array. Since this morphological development of the interface causes segregation of dopants, great interest in understanding the pattern formation in faceted cellular array growth has been taken [1-3]. Although many theoretical models have been proposed, *e.g.*, two-dimensional nuclei [4, 5], persistent dislocation [6] and accumulated strain energy [7], there have been few works that experimental evidences are consistent with theoretical mechanisms. Shangguan *et al.* performed in situ observations of unidirectional solidification of transparent and faceting organic compounds by a microscope and by numerical work on the pattern formation [8]. In their studies, it has been suggested that the mechanism to maintain stable morphology of the interface at the steady-state growth rate imposed by the heater movement was attributed to solute pile-up in front of the bottom of the cellular interface, and solute concentration at the bottom increased to keep constant kinetic undercooling. This was based on the assumption that even in materials characterized by faceted solidification the latent heat of solidification was quickly removed through the solid.

Higashino *et al.* reported appearance of recalescence regions in front of growing surface in salol by means of an in situ observation using an interferometer [9]. In addition, they observed that the morphology of the cellular array was kept at constant growth rate, although purified salol was used as a specimen. The growth rate and the temperature gradient in the cell were same orders of magnitude as the Shangguan's works. The main reason of the discrepancy between the theories and the experimental results is that it is difficult to quantitatively evaluate the interface kinetics effect, which controls incorporation process of atoms or molecules at the interface. However, temperature and concentration gradients in the liquid become driving forces of convection in the liquid and the convection influences the morphological change of the S/L interface. Therefore, application of a microgravity environment is considered to be a promising method to investigate the morphological stability of the S/L interface. In the present paper two visualization experiments in microgravity for crystal growth of model transparent material having a faceted interface are briefly introduced.

2. Experimental Procedure

2.1 Specimen

In the space experiments using a sounding rocket and the International Space Station (ISS) crystallization of salol (phenyl salicylate) - *t*-butyl alcohol alloy and purified salol, which show faceted growth interfaces, will be carried out with a constant temperature gradient G_T and with a constant cooling rate R_C at both ends of the specimen cell. These materials of commercial grade of 98 wt% are distilled or purified by several zone-refining cycles on a laboratory scale, because measuring error due to undesirable impurity in the material should be eliminated for the interferometric analysis described below. A binary phase diagram of the alloy was shown in Ref. [10].

The specimen cell consists of a quartz glass container, Peltier devices, thermocouples, and the specimen material. The specimen is enclosed into the glass container. Two thin thermocouples are installed in the container to obtain reference temperature in the specimen. The Peltier devices embedded at the both ends of the specimen cell for heating and cooling are controlled by the pair of the thermocouples, embedded in the metal blocks [10]. The thickness of the specimen is 1 mm in order to suppress buoyancy convection driven by the residual gravity acceleration and to

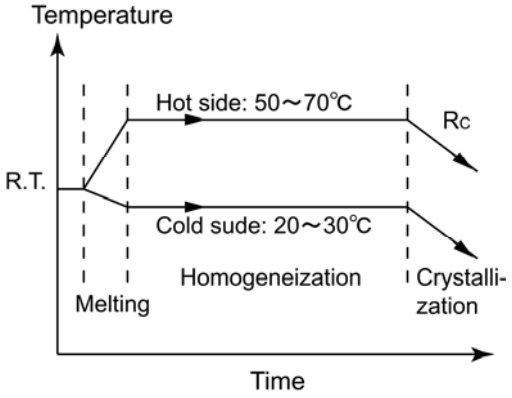

Fig. 1 Temperature program of specimen cell.

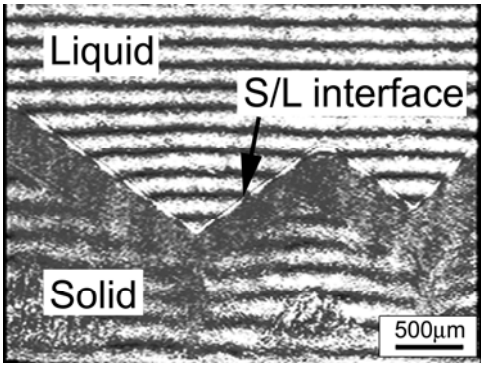

Fig. 2 Interference fringe pattern at S/L interface of purified salol.

measure temperature and concentration fields by an in situ observation setup.

A typical temperature program for controlling crystallization of the specimen is shown in **Fig. 1**. To preset initial boundary spacing in the crystals, seed crystals with a favorable orientation are pre-grown in several pores of 500 μmϕ in the bottom plate of the cell at the first stage so that cell boundaries are isolated at regular intervals. In the second stage, periodic remelting and regrowth during the growth of seed crystals are performed to improve the quality of crystals. At the beginning of crystallization, the specimen is kept stationary in temperature gradient for several hours, so that a planar S/L interface is formed and the seed crystals grown up to nearly constant dimensions.

2.2 Basis of in situ observation

Refractive index of transparent alloy melt depends on temperature, concentration and wavelength of incident light. If change of temperature and concentration in the melt, ΔT and ΔC, are small enough, change of the refractive index Δn_i satisfies the following linear relation:

$$\Delta n_i = \left(\partial n_i / \partial T\right)_C \Delta T + \left(\partial n_i / \partial C\right)_T \Delta C \quad ,(1)$$

where the subscript i: wavelength of light, n_i: refractive index of melt; T: temperature; and C: concentration, respectively. Therefore, spatial distribution images of two different wavelengths are transformed into temperature and concentration distributions by solving Eq. (1). In the temperature range from 298K to 338K, $\left(\partial n_i / \partial T\right)_{TC}$ and $\left(\partial n_i / \partial C\right)_C$ of salol - *t*-butyl alcohol were experimentally obtained for λ = 458nm and 780nm in wavelength [10].

Two-wavelength microscopic interferometers based on the above principle will be used in order to visualize both the refractive index distributions in the liquid as interference fringes and the morphological change of the S/L interface as bright field images. **Fig. 2** shows an example image of an interference fringe pattern in the vicinity of the S/L interface with λ = 458 nm.

2.3 Numerical calculation of latent heat effect on temperature in specimen

Temperature and concentration gradients in the vicinity of an S/L interface are known as the important factors to control the morphological instability of the interface. Released latent heat accompanied with solidification is removed quickly through the solid as in metallic material, and the temperature gradient in liquid is the kept almost constant even close to the S/L interface. However, the latent heat for faceting material is in general large enough to influence the temperature field in the liquid. Therefore, temperature profile in the specimen is necessary to estimated by a numerical simulation in order to determine cooling rate and temperature gradient of the specimen cell for microgravity experiments. Therefore, temperature raise caused by release of latent heat in the vicinity of the S/L interface was estimated under the steady state condition by taking account of heat flow in the glass container.

The simplified configuration for the material in the glass container and the coordinate system are illustrated in **Fig. 3**. Each apex of the sawtooth-shape S/L interface is fixed to be 60 degrees. Energy equations for liquid, solid and glass in the steady state associated with a translating coordinate system are expressed in form as follows:

$$\alpha_j \nabla^2 T + (\boldsymbol{V} \cdot \nabla) T = 0 \,, \qquad (2)$$

where α_j, thermal diffusivity; the subscript j, liquid, solid and glass; and $\boldsymbol{V}$ = (0, 0, V_0), translation velocity vector along the z-axis, respectively. The translation velocity V_0 corresponding to growth rate of crystal is a function of cooling rate R_C and temperature gradient G_T in the steady state as:

$$V_0 = R_C / G_T \,. \qquad (3)$$

The boundary conditions are as follows:

$$\left(\kappa_S \nabla T\big|_{\text{solid}} - \kappa_L \nabla T\big|_{\text{liquid}}\right) \cdot \boldsymbol{n} = Q V_0$$

for S/L interface, (4a)

$$T = G_T z + T_0 \quad \text{for glass wall,} \qquad (4b)$$

$$T = T_0 \quad \text{for } Z = 0, \qquad (4c)$$

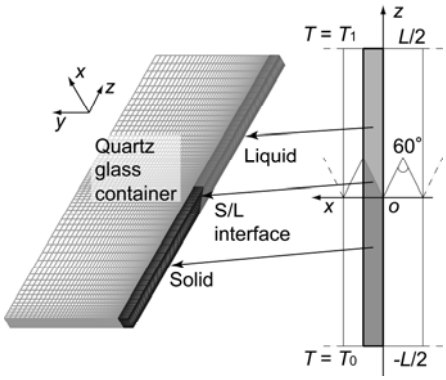

Fig. 3 Model of specimen container.

Table 1 Parameters used in numerical simulation.

Symbol	Value	Unit	Ref.
R_C	0.05, 0.2, 0.5, 1, 2	K/min	-
G_T	$7x10^2$, $1.5x10^3$	K/m	-
L	$1.6x10^{-2}$	m	-
α_G	$7.7x10^{-7}$	m^2/s	-
α_L	$9.65x10^{-8}$	m^2/s	[12]
α_S	$1.65x10^{-7}$	m^2/s	[12]
κ_G	1.5	W/m K	-
κ_L	0.180	W/m K	[12]
$\kappa\Sigma$	0.251	W/m K	[12]
Θ	1.2x108	J/ m3	[12]

$$T = T_1 \qquad \text{for } Z = L, \qquad (4d)$$

where κ_S and κ_L, thermal conductivity of sold and liquid; $\boldsymbol{n}$, unit normal vector to S/L interface; Q, latent heat; T_0 and T_1, temperature at cold and hot sides; and L, liquid length, respectively. The right term of Eq. (4a) expresses the effect of latent heat at the interface. Concentration dependency of the latent heat was neglected for simplicity. Numerical simulations for the temperature field were performed using the commercial software package FIDAP 8.7.2 [11], which was based on the finite element method. All calculations were carried out with a nonuniform four-node quadrilateral element mesh for liquid. The parameters used in the numerical simulation are shown in **Table 1**.

Fig. 4 shows the calculated results of temperature profiles along the *z*-axis, where the temperature and the distance were normalized as $T_N = (T-T_0)/(T_1-T_0)$ and $Z_N = z/L$, respectively. The temperature gradient ahead of the S/L interface becomes negative value from positive one with the increase of R_C or with the decrease of G_T, whereas the temperature gradient is positive value for low V_0. The values of R_C and G_T in Table 1 will be used in the ISS experiment as mentioned in Section 3.2.

3. Onboard Setup for Space Experiments

A drop shaft facility did not provide sufficient experiment time for observing the crystal growth of the faceted cellular array growth [13]. To obtain longer duration of microgravity, two space flight opportunities,

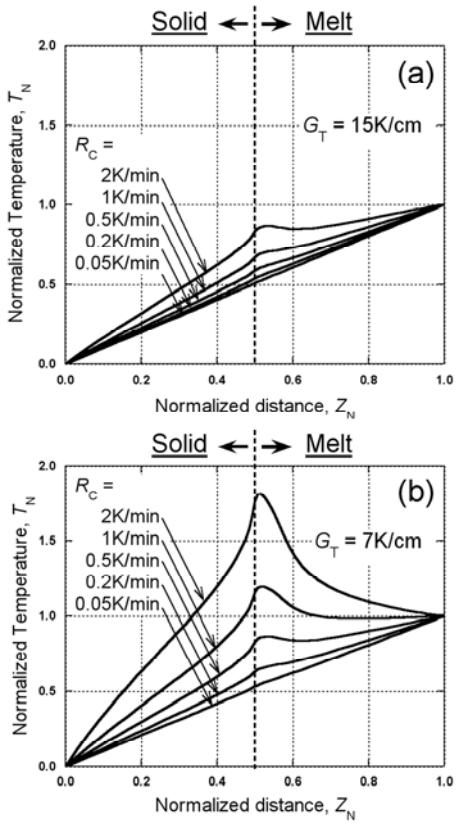

Fig. 4 Numerical result of temperature profile along *z*-axis of specimen cell in Fig. 3.

a sounding rocket and ISS, will be utilized to investigate the growth. In this section the onboard setup for the space experiments are described.

3.1 S-520 #24 experiment

A single stage sounding rocket, S-520, has been developed and launched by Institute of Space and Astronautical Science (ISAS) and contributed to scientific researches. The rocket has a flexible payload capability of 100 kg with 520 mm diameter and provides more than 5 minutes for a microgravity environment in its free-fall flight. Especially S-520 #24 is planned to be launched at Kagoshima Space Center in summer of 2008 as a vehicle for two microgravity experiments: (a) in situ observation of faceted crystal growth, and (b) diamond synthesis from a gas phase.

Required characteristics of setups used in a sounding rocket are commonly small in mass and stable mechanically against external disturbances and small power dissipations. From these standpoints, a common-path type microscopic interferometer with the same design as SFU/MEX [14], as shown in **Fig. 5**, will be mounted in the rocket. The optical principle of the present interference is based on the idea of the lens interferometer proposed by Dyson [15]. Light sources of the present system are laser diodes with λ = 780 nm and 680 nm, and the power dissipation of the system is at most 3 W. Robustness of the interferometer against the space environment was demonstrated in the SFU

mission [14].

In the crystal growth experiment purified salol will be used as a specimen for utilization of the microgravity duration of 5 minutes. Now manufacturing of the other onboard components, a filling process of specimen into the container, and determination of temperature program are pushed forward.

3.2. International Space Station experiment

The advantages of ISS over a parabolic flight of a sounding rocket are as follows: 1) achievement of a longer and high quality microgravity environment, (2) ability of experimental operations by the ISS crew or remotely by the experiment rack. Experiment parameters can be changed by sending commands from Earth. Solution Crystallization Observation Facility (SCOF) is a Japan Aerospace Exploration Agency (JAXA) subrack facility. SCOF is scheduled for launch inside the Ryutai Experiment Rack to ISS on the space shuttle. SCOF has an amplitude modulation microscope and is equipped with two-wavelength microscopic interferometer with λ = 532 nm and 780 nm to simultaneously measure morphological change of S/L interface and distributions of temperature and concentration fields in the melt.

Two specimen cells with different concentration of *t*-butyl alcohol are placed in a cell cartridge with 220 mm in diameter and 65 mm in height. The cell cartridge is available with temperature, pressure and atmosphere controls. The specimens will be partially melted and crystallized in the same specimen cell with different temperature program repeatedly. The initial concentration of *t*-butyl alcohol in the melt will be 4 mol% and 8 mol%. Preparation process of the seed crystal in the cell is now being evaluated in the ground experiments. The experimental operation of SCOF is scheduled in 2008.

4. Summary

Two visualization experiments for faceted cellular array growth in microgravity, which are scheduled to be performed in 2008, were briefly introduced from the viewpoint of the observation method and the specimen preparation. In these experiments temperature and concentration fields in the vicinity of the S/L interface in the faceted growth will be simultaneously measured in real time in order to reveal the morphological instability of the interface. The in situ observation setup onboard S-520 #24 has been developed, and some ground experiments are processed to determine the temperature program for the crystallization. For the ISS experiment, development of the onboard setups has been finished and the preparation process of the seed crystal is being evaluated.

Acknowledgements

The authors would like to express their sincere thanks to Dr. T. Shimaoka of Japan Space forum for his technical support.

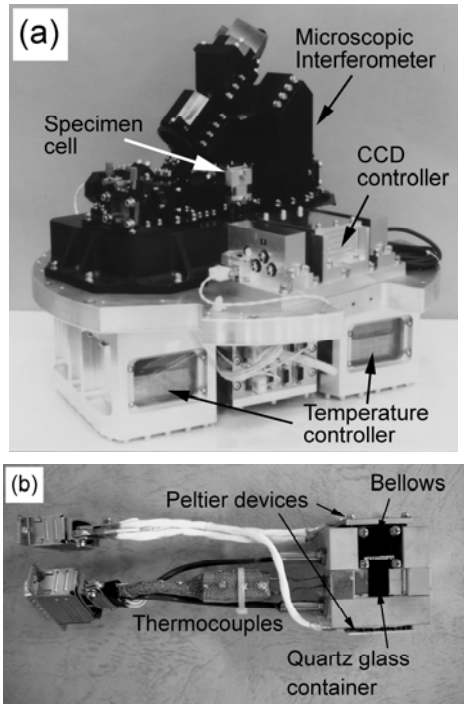

Fig. 5 In situ observation setup for crystal growth onboard S-520 #24: (a) microscopic interferometer, (b) specimen cell.

References

1) Maby, E.W., Geis, M.W., LeCoz, Y.L., Silversmith, D.J., Mountain, R.W., and Antoniadis, D.A., Electron. Device Lett., **edl-2**, 241, 1981.
2) Geis, M.W., Smith, H.I., Tsaur, B-Y, Fan, J.C.C., Silversmith, D.J., and Mountain, R.W., *J. Electrochem. Soc.,* **129**, 2813, 1982.
3) Pfeiffer, L., Paine, S., Gilmer, G.H., Saarloos, W. van, and West, K.W., *Phys. Rev. Lett.*, **54**, 1944, 1985.
4) Cahn, J. W., Hilling, W.B., and Sears, G.W., *Acta Met.,***12**, 1421, 1964.
5) Jackson, K.A., Uhlmann, D.R., and Hunt, J.D., *J. Crystal Growth*, **1**, 1, 1967.
6) Morrss, P.J., Kirtisinghe, D., Strickland-Constable, R.F., *J. Crystal Growth*, **2**, 97, 1968.
7) Dey, N., and Sekhar, J.A., *Acta Metall. Mate.,* **41**, 409, 1993.
8) Shangguan, D.K. and Hunt, J.D., *Metall. Trans. A*, **23A**, 1111, 1992.
9) Higashino, T., Inatomi, Y., and Kuribayashi, K., *J. Crystal Growth*, **128**, 178, 1993.
10) Yoshida, T., Inatomi, Y., and Kuribayashi, K., *Trans. Mat. Soc. Jpn.,* **16A**, 637, 1994.
11) Engelman, M.S., FIDAP 8.0, Fluent Inc., Lebanon, NH, USA, 1998.
12) Dürig, U., Bilgram, J.H., and Känzig, W., *Phys. Rev. A.*, **30**, 946, 1984.
13) Inatomi, Y., Yoshida, T., and Kuribayashi, K., *Microgravity Q.*, **3**, 93, 1993.
14) Kuribayashi, K., Sato, E., and Inatomi, Y., *Proc. 4th Int. conf. of TMS*, p.43, 1992.
15) Dyson, J., *J. Opt. Soc. Am.,* **53**, 690, 1963.